Polymer 162 (2019) 80–90

Contents lists available at ScienceDirect

Polymer

journal homepage: www.elsevier.com/locate/polymer

Surface modification of PVA hydrogel membranes with carboxybetaine methacrylate via PET-RAFT for anti-fouling

Yanming Lin[a,1], Ling Wang[c,d,1], Jinsheng Zhou[b], Lin Ye[c,d], Huiyuan Hu[a], Zhongkuan Luo[a,b], Li Zhou[a,*]

[a] College of Chemistry and Environmental Engineering, Shenzhen University, No. 3688 Nanhai Road, Nanshan District, Shenzhen, Guangdong Province, China
[b] School of Material Science and Engineering, Zhejiang University, Hangzhou, China
[c] Shenzhen Key Laboratory of Ophthalmology, Shenzhen Eye Hospital, ShenZhen, Guangdong, China
[d] School of Ophthalmology& Optometry Affiliated to Shenzhen University, Shenzhen, 518040, Guangdong, China

HIGHLIGHTS

- The PET-RAFT is first used in surface modification of PVA hydrogel membrane and it has a large industrial application potential.
- We use a low-cost organic dyes Eosin Y as photoredox catalyst and investigated some PET-RAFT reaction factors to research the reaction mechanism.
- We obtained the relationship of grafting ratio and the weight of elements.
- We synthesized a kind of zwitterionic— Carboxybetaine Methacrylate(CBMA).
- We further enhanced the anti-fouling capacity of PVA hydrogel membrane via pCBMA grafting.

ARTICLE INFO

Keywords:
polyvinyl alcohol (PVA)
Carboxybetaine methacrylate (CBMA)
Photoinduced electron transfer-reversible addition-fragmentation chain transfer polymerization (PET-RAFT)
Anti-adhesion
Cytotoxicity

ABSTRACT

In this study, we grafted brush-like CBMA copolymer brushes onto the surface of PVA hydrogel membrane through photo-induced electron transfer–reversible addition fragmentation chain transfer (PET-RAFT) polymerization. ATR-FTIR, XPS, AFM, UV–Vis absorption spectra and elemental analysis were adopted to characterize the hydrogels, and equilibrium swelling, water contact angle, vitro cytotoxicity assay, protein adsorption and cells adhesion experiments were used to evaluate the related property of hydrogels. The results of ATR-FTIR and XPS showed that pCBMA was successfully grafted onto the surface of PVA hydrogel membrane. The Ra roughness of hydrogel surface in AFM increased slightly from 5.44 nm to 6.12 nm. Transmittance of the PVA-g-pCBMA hydrogel in the visible range (380 nm-780 nm) was remaining at 91.2%–97.0%. The optimal reaction conditions (CPADB: 1.20 mmol/L, Eosin Y: 0.03 mmol/L and CBMA: 358 mmol/L) were confirmed through control experiments. The equilibrium swelling and water contact angle showed that the swelling ratio increased from 2.06 $cm^3 g^{-1}$ to 3.65 $cm^3 g^{-1}$, while the water contact angle decreased from 45.94° to 18.06° with the increase of grafting ratio (23.92%–55.18%). In vitro cytotoxicity assay by CCK-8 showed that the cells relative viability remained at least 90.55%. Anti-protein adsorption experiment illustrated approximately 57.2% improvement of anti-protein capacity at 37 °C, while cells adhesion experiment also showed about 64.57% improvement of anti-cells capacity. These results revealed the applicability of the oxygen tolerant PET-RAFT mechanism on the PVA modification and it was effective, feasible and non-cytotoxic method to prepare the other functional PVA hydrogel membrane.

1. Introduction

Polyvinyl alcohol (PVA) has excellent biocompatibility, significant stability and similarity moisture content to human tissues [1–7]. Hydrogels are considered as promising scaffolds for cell encapsulation and tissue regeneration [7–9]. And PVA based hydrogel has promising applications in biomedical material, such as drug delivery system, biosensor, artificial cartilage, anti-coagulation materials, biomedical

* Corresponding author.
E-mail addresses: Yanming_lam@yeah.net (Y. Lin), wangl972@163.com (L. Wang), zhouli_2050@163.com (L. Zhou).
[1] These authors contributed equally to this work and should be considered co-first authors. She is responsible for the in vitro cytotoxicity and cell adhesion experiment.

https://doi.org/10.1016/j.polymer.2018.12.026
Received 6 September 2018; Received in revised form 6 December 2018; Accepted 16 December 2018
Available online 26 December 2018
0032-3861/ © 2018 Published by Elsevier Ltd.

sponge, artificial cornea [3,7,10]. Nevertheless, the formation of biofilm caused by the cells specific adsorption and the proteins nonspecific adsorption onto the implanted biomaterials, is one of the common complications for these biomedical devices and limits its application [11–14]. From bionics, surface modification with antifouling self-assembled monolayers (SAMs) or polymers is efficacious to resist nonspecific protein adsorption [15–17].

In recent years, anti-fouling mechanism of zwitterionic material has been investigated deeply through experiment and molecular simulations. And researchers hold that, the hydration layer is a barrier to protein adsorption which attached by electrostatic interaction of opposite charge in the zwitterionic material [18–21].

Zwitterionic polymer based on phospholipid bilayer structure can restrain bio-fouling of protein and bacteria [22]. Many grafting strategies have been investigated. Pingsheng Liu et al. [23] grafted three kinds of zwitterionic polymers onto cellulose via SI-ATRP. Dangsheng Xiong et al. [24] grafted brush-like structure of MPC onto polyethylene via UV radiation, in order to acquire ultra-low friction coefficients which close to the natural joints. Shaoyi Jiang et al. [25–27] has reported the application of zwitterionic in improving anti-fouling performance. Therefore, zwitterionic polymer modification is the most effective method for anti-fouling.

Since 1998, Rizzardo [28] first reported a new method of free radical polymerization called reversible addition-fragmentation chain transfer (RAFT), RAFT polymerization has been widely used to prepare of high polymers and specific structural polymers, and surface modification [29,30]. Cyrille Boyer researched the RAFT polymerization deeply and found a highly efficient photo-induced electron transfer-RAFT (PET-RAFT) polymerization using metallo- and organo-photocatalysts [31–34]. PET-RAFT polymerization process can react under mild conditions, such as visible light-mediated, low temperature, controllable and oxygen tolerable. Also, it has been verified that organo-photocatalysts with different absorption is efficient in PET-RAFT.

Researchers have utilized RAFT polymerization on surface modification [35–39], but only a little research has been reported about PET-RAFT. In this paper, we demonstrated the applicability of the oxygen tolerant PET-RAFT mechanism on the PVA modification. Scheme 1 shows the proposed reaction mechanism of PVA hydrogel membrane modification via PET-RAFT polymerization system. Zwitterionic monomer CBMA was directly grafted onto PVA hydrogel membrane surface via PET-RAFT polymerization, using eosin Y as photo redox catalyst. The ATR-FTIR and XPS were used to analyze the surface chemical compositions of modified PVA hydrogel membrane. The elemental analyzer was used to measure the whole chemical compositions of modified PVA hydrogel membrane to evaluate the reaction factors. And the hydrophilicity of PVA hydrogel membrane was characterized by the swelling equilibrium test and water contact angle. Subsequently, the biocompatibility of sample was evaluated by CCK-8 assay. Finally, the adhesion resistance properties were evaluated by anti-cell adhesion and anti-protein adsorption in vitro.

2. Experiment

2.1. Materials

Polyvinyl Alcohol (PVA, 1750 ± 50, China National Pharmaceutical Group); Dimethyl-aminoethyl methacrylate (DMAEMA, 99%, Aladdin); 4-Cyano-4-(phenyl-carbonothioylthio) pentanoic acid (CPADB, ≥97%, Sigma-Aldrich); Phosphate Buffered Saline (PBS, Hyclone); N, N-dimethyl formamide (DMF, 99.5%, Macklin); acrylic acid (99%, Macklin); 4-methoxyphenol (GC, ≥99.8%, Macklin); Eosin Y water solution (EY, Biological stain, Macklin); Triethylamine (TEA, 99%, Macklin); Bovine Serum Albumin BSA-V (biological stain, Macklin); Sodium dodecyl sulphate (SDS, 98%, Macklin).

2.2. Preparation of hydrogel membrane and CBMA

2.2.1. Preparation of carboxybetaine methacrylate (CBMA)

The carboxybetaine methacrylate (CBMA) was prepared mainly according to a patent invented by Yuting Li [40]. Acrylic acid (14 ml) was added slowly into a three-necked flask with DMAEMA (17 ml) and 4-methoxy phenol (0.02 g) at 0 °C, stirred with agitator blade and react for 4 h in room-temperature until solution thickens; next, 10 ml acetone was added for dilution and stirred for 24 h. After reaction, CBMA was precipitated with 50 ml triethylamine and purified with acetone for three times, white powder production was dried in vacuum and carboxybetaine methacrylate (CBMA) was prepared (productivity ≈ 75%). ^{1}H NMR was detected on Bruker spectrometer (400 MHz) and shown in supplementary information. For CBMA (in D_2O): δ6.01 ppm (s, 1H, cis, =CH), δ5.63 ppm (s, 1H, trans, =CH), δ4.50 ppm (s, 2H, $-CH_2-O$), δ3.67 ppm (t, 2H, $-CH_2-$), δ3.54 ppm (t, 2H, $-CH_2-$), δ3.06 ppm (s, 6H, $N-CH_3$), δ2.61, ppm (t, 2H, $-CH_2-$), δ1.80 ppm (s, 3H, $-CH_3$).

2.2.2. Preparation of PVA hydrogel membrane

Firstly, PVA-1750 ± 50 (4 g) was swelled in a mixed solvent (16 ml DMSO and 4 ml H_2O) at 65 °C for 1 h, 75 °C for 4 h and 95 °C for 10 h until PVA dissolved as a viscous fluid. Then, the viscous PVA fluid was poured into a mold (80 mm × 80 mm × 2 mm) and then frozen at −20 °C. After six freeze-thaw cycles, PVA hydrogel membrane was soaked in distilled water. Finally, PVA hydrogel membranes were prepared.

2.2.3. Surface grafting of PVA hydrogel membrane with pCBMA via PET-RAFT

CPADB and eosin Y water solution (EY) were dissolved in DMF to prepare 0.01 mol/L and 0.005 mol/L solutions, respectively. PVA hydrogel membranes were cut into a circle shape (d ≈ 10 mm) and a strip shape (10 mm × 40 mm) via CO_2 laser cutter.

CBMA (0.5 g-3.5 g) were dissolved in 63% DMF aqueous solution and mixed with CPADB solution (0.05–4.85 ml), Eosin Y solution (0.1–1.9 ml) and triethylamine (TEA, 5 ml) as a modifying solution. TEA can reduce oxygen in PET-RAFT polymerization [31].

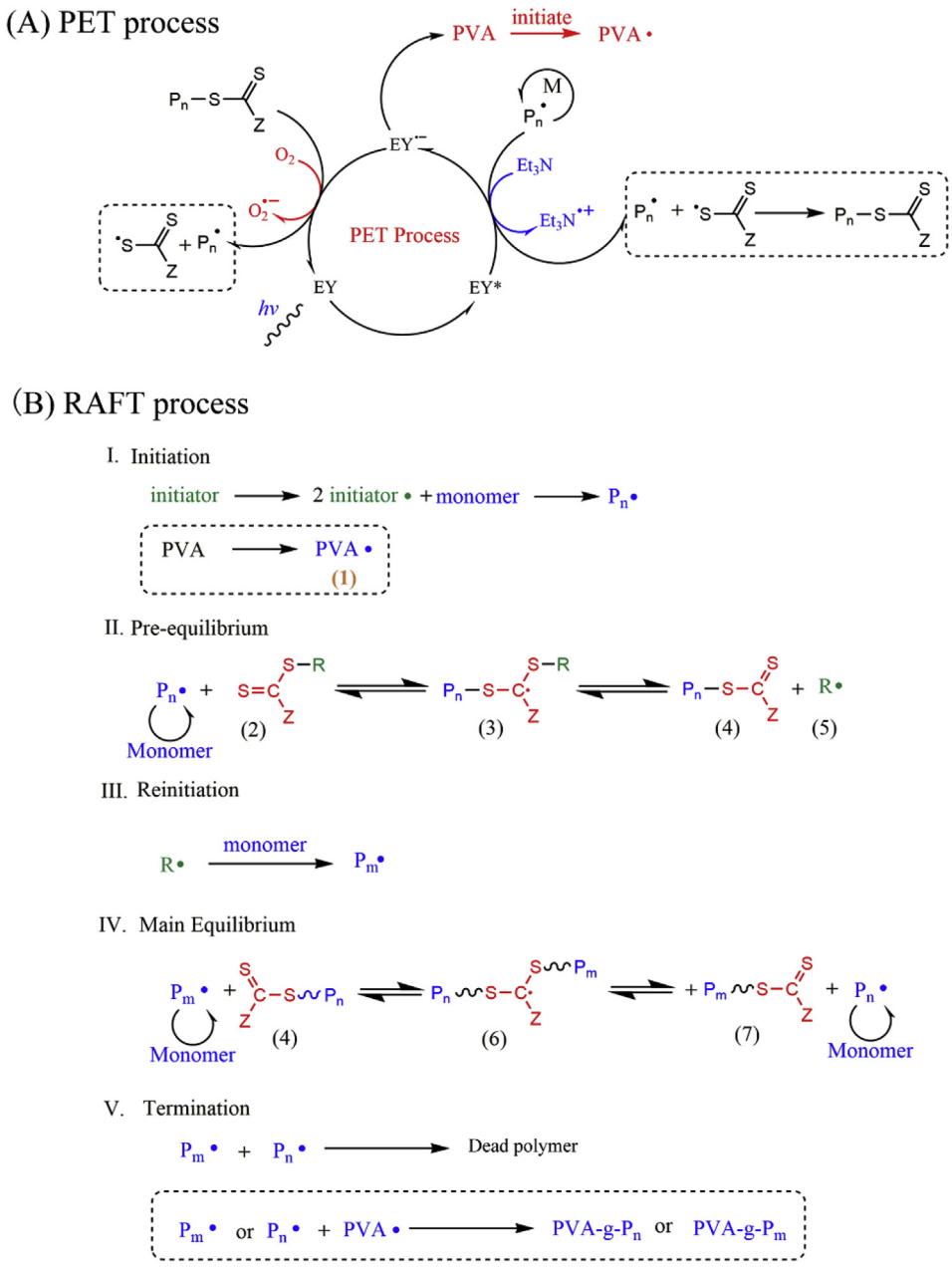
PVA hydrogel membranes were put into the modifying solution in 35 ml vials. The modification process performed at 30 °C and blue LED light (450–460 nm) for 10 h in a gas bath the rmostatic shaker. After modification, the modified PVA (PVA-g-pCBMA) hydrogel membranes were removed from the vials. PVA-g-pCBMA hydrogel membrane was cleaned by ultrasonic and soaked in deionized water for 5 days (changed the deionized water three times per day).

2.3. Characterization of hydrogel membranes

ATR-FTIR spectra was detected by an FTIR instrument with Quest ATR accessory (IR Affinity-1, Perkin Elmer) in the 4000–400 cm^{-1} frequency range in steps of 4 cm^{-1}. The surface atomic compositions of membranes were detected by X-ray photoelectron spectroscopy (XPS, Thermo Scientific Escalab 250Xi, tube voltage = 15 kV, tube current = 12 mA, diameter beam spot = 500 μm) with Al Kα excitation radiation (hν = 1486.6 eV). Surface microstructure (3 × 3 μm and 1 × 1 μm) was detected by atomic force microscope (MultiMode 8). The transmittances of the hydrogel membranes were measured by using a Shimadzu UV–visible light absorption spectroscope (UV-2550) produced by Shimadzu. Thermogravimetric analysis (TGA) of hydrogel membrane samples were performed on a Hot Sync Analyzer (STA409PC, NETZSCH-Geratebau GmbH), nitrogen atmosphere, 10 °C·min^{-1}.

2.4. Reaction factors

Several control experiments were carried out to investigate the reaction, including monomers content, catalyst content and chain transfer



Scheme 1. Proposed mechanism of oxygen tolerant PET-RAFT on the PVA modification.

agent content. The elemental contents of nitrogen of samples were examined by elemental analyzer to evaluate the effect of a single condition (Elementar, vario EL cube).

In order to reflect the extent of grafting visually and to evaluate the relationship between nitrogen element content and grafting level, percentage of grafting was calculated through quality change, and the nitrogen element content of corresponding sample was test through element analysis. The percentage of grafting (*Gp*) is determined by the formula

$$Gp = \frac{m_g - m_0}{m_0} \times 100\% \quad (1)$$

Where m_g and m_0 are the weights of the PVA-g-pCBMA and PVA hydrogel membranes in a dry state, respectively.2.5 Hydrophilicity measurements.

In swelling equilibrium tests, samples (size around 10 mm × 40 mm and thickness around 2 mm) were frozen and dried to constant weight (m_0), then immersed into distilled water and swelled until equilibrium at 25 °C.

After designated periods of time, the samples were taken out of water, removed the excess water, weighted and recorded as m_t, and then returned to water. The average degree of swelling Q_t is determined by the formula

$$Q_t = \frac{V_0}{m_0} = \frac{(m_t - m_0)/\rho}{m_0} \quad (2)$$

Where m_t and m_0 are the weights of the swollen and dried hydrogels, respectively. V_0 is the value of water absorbed in hydrogel. ρ is the Solvent density ($g{\cdot}cm^{-3}$).

The water content W_∞ is determined by the formula

$$W_\infty = \frac{m_\infty - m_0}{m_\infty} \times 100\% \quad (3)$$

Where m_∞ is the final weight of swollen hydrogels, m_0 is the weight of dried hydrogels.

The water contact angle of hydrogel membrane (remain hydrous)

was measured by the contact angle measuring instrument (JC2000C1) produced by POWEREACH.

2.5. Cytotoxicity and anti-fouling experiments

2.5.1. Protein adsorption experiment

BSA (5 mg/ml) were selected to conduct protein adsorption experiments. The PVA hydrogel membranes were incubated in 99.5% ethanol for 2 h, then equilibrated in phosphate buffer (pH = 7.4, 25 °C and 37 °C) for 4 h. Finally, samples immersed in BSA protein solutions at 25 °C and 37 °C for 4 h.

Afterward, samples were gently washed for three times with PBS, soaked and oscillated in SDS (1 wt%, water solution, 37 °C) for 4 h. The protein concentrations in the solutions were quantified by Micro BCA™ protein assay reagent kits using an Ultra-micro Microplate Spectrophotometer (Epoch) at a wavelength of 562 nm. 5 parallel holes in 96-well plate.

2.5.2. Cytotoxicity

To evaluate the biocompatibility of materials, we test the cytotoxicity though CCK-8 assay which is a method for cell viability detective with significant sensitivity and reproducibility.

Before the experiment, the samples (circle shape, d ≈ 10 mm) were treated with gamma ray (^{60}Co as a radioactive source) sterilization and immersed in 2 ml serum-free DMEM medium for 24 h. After pre-treatment, the samples were immersed in 1 ml of 8% FBS DMEM medium, respectively. The cells (Eyelid fibroblasts) were seeded in 12-well plates (1×10^5 cells/ml) and incubated for 24 h. After that, the supernatant and materials were discarded, and 0.5 ml/well CCK-8 reagent (DMEM: CCK-8 reagent = 10:1) was added and incubated for 1 h. 100 μl/well supernatant (4 in parallel, 400 μl in total) added in 96-well plate. Optical density (O.D.) values were detected by micro-plate reader at 450 nm. The cells relative viability (CRV) was calculated by the equation.

$$CRV = \frac{O.D._{test}}{O.D._{control}} \times 100\% \quad (4)$$

2.5.3. Anti-cell adhesion

In order to obtain the statistical data for the cell adhesion, cell count standard curve was made. Cell suspension with different concentrations were prepared, and then 0.5 ml/well CCK-8 reagent (DMEM: CCK-8 reagent = 10:1) was added and incubated for 1 h. Finally, optical density (O.D.) values were detected by micro-plate reader at 450 nm and the cell count standard curve completed.

CCK-8 assay was also used to assess the anti-cell adhesion properties. The cell (eyelid fibroblasts) and samples were treated as above process. After incubated for 1, 3, 5, 7 days, the materials were gently rinsed 3 times with PBS and fixed with 4% paraformaldehyde. Cells adhered to the membrane surface were inspected via SEM (HITACHI, S−3400N(II)) after freeze-dried.

3. Results and discussion

3.1. Proposed reaction mechanism

The proposed mechanism of PET-RAFT polymerization is outlined in Scheme 1. It can be divided into two parts, photo-induced electron/energy transfer (PET) and traditional RAFT process.

Organo-photocatalyst such as eosin Y has high redox potentials with a long lifetime of excited states [31,41]. The triplet state of eosin Y has strong reducing (E^*_{red} ($PC^*/PC^{\bullet-}$) = +1.18 V *vs.* SCE (standard calomel electrode)) and oxidizing (E^*_{red} ($PC^{\bullet+}/PC^*$) = −1.60 V *vs.* SCE) potentials [31]. In PET process (Scheme 1(A)), firstly, eosin Y transformed from ground state to a triplet excited state (EY*) under the visible light. Then, with the present of an electron donor (Et_3N), an electron is transferred from Et_3N to EY*, meanwhile, Et_3N generate $Et_3N^{\bullet+}$ and EY* generate an EY radical anion ($EY^{\bullet-}$) [42]. Finally, one part of EY radical anion ($EY^{\bullet-}$) reduced O_2 to generate superoxide ($O_2^{\bullet-}$) while another fraction of $EY^{\bullet-}$ transferred an electron to CPADB to generate a propagating radical ($Pn^{\bullet}$) for chain growth [33,34,41,43].

Alcohols are ideal precursors of alkoxy radicals [44,45]. However, the formation of alkoxy radicals by homogenization of alcohols requires high energy. Alcohol is usually oxidized to produce alkoxy radicals under the activation of transition metals and strong oxidation conditions [46–48]. PET process is actually a redox process, PVA chain is oxidized to produce alkoxy radicals and generate $PVA^{\bullet}$.

RAFT process includes five period shown as Scheme 1(B), the traditional initiation stage is instead by PET process mentioned above [49]; And in the pre-equilibrium stage, a propagating radical ($Pn^{\bullet}$) react with CPADB (2) to form a radical intermediate (3), then divide into another thiocarbonylthio group (4) and a new radical ($R^{\bullet}$) (5); And radical ($R^{\bullet}$) may react with monomer to form a new propagating radical ($Pm^{\bullet}$), called re-initiation [41,43]; Next, after the initial CPADB is consumed, 'main equilibrium' of activation-deactivation is established, and in this stage, monomer will keep initiating and molecular weight of $Pn^{\bullet}$ keep increasing [43,50]. It is similar to chain growth stage in traditional radical polymerization; Termination is inescapable, it includes two parts and the combination between radical ($Pn^{\bullet}$) and $PVA^{\bullet}$ is the ultimate aim.

3.2. Reaction factors

Elemental analysis is an effective method to evaluate the amount of grafted and investigate the reaction mechanism. The nitrogen contents were used. Fig. 1(a) shows that the nitrogen content of PVA-g-pCBMA hydrogel membrane increased and then became steady with the increased concentration of grafting CBMA (up to 358 mmol/L). As shown in Scheme 1, the grafting reaction is largely affected by the termination stage. We hope termination reacts between radical ($Pn^{\bullet}$) and $PVA^{\bullet}$ but another route is unavoidable [50].

Herein, a non-negligible phenomenon of reaction is the formation of transparent gels. As shown in Scheme 1(B), termination reactions are inescapable when molecular weight increases gradually and CPADB does not adequately control the polymerization of a given monomer [50]. With the increasing content of CBMA, termination between propagating radicals ($Pm^{\bullet}$ or $Pn^{\bullet}$) becomes more probable. It leads an evident phenomenon that formation of transparent gels. Therefore, we can see the nitrogen content becomes steady.

The content of photocatalyst (EY) (Fig. 1(b)) and CPADB (Fig. 1(c)) are significant to the reaction process. In PET process, the initiation of monomer in solution phase goes easier than solid-liquid interface of PVA hydrogel, besides, the amount of free radical sites at the solid-liquid interface are limited.

On one hand, with increasing content of photocatalyst, PET process accelerated, more monomers were initiated and the 'main equilibrium' comes earlier [33,51]. The concentrations of propagating radicals increased but $PVA^{\bullet}$ did not. On the other hand, with increasing content of CPADB, 'pre-equilibrium' stage prolong [33,34,51], we can see an improvement of nitrogen content at low concentration range of CPADB (0–1.20 mmol/L). However, the further increasing concentration of CPADB (1.20–7.00 mmol/L) also leads the increasing of propagating radicals while $PVA^{\bullet}$ did not. And termination between propagating radicals ($Pm^{\bullet}$ or $Pn^{\bullet}$) becomes more probable at high radical concentrations [50]. Therefore, the results are both showed a downward trend with the increasing content of EY and CPADB.

According to the results, we obtained efficient concentrations of CTA and photocatalyst. And the ratio of them is around 40:1, which is consistent with some report [31]. Photo-catalyst concentration could be reduced to 0.03 mmol/L even in the presence of oxygen.

The appearance of element nitrogen indicates the zwitterionic pCBMA has been grafted on the surface of PVA hydrogel membrane

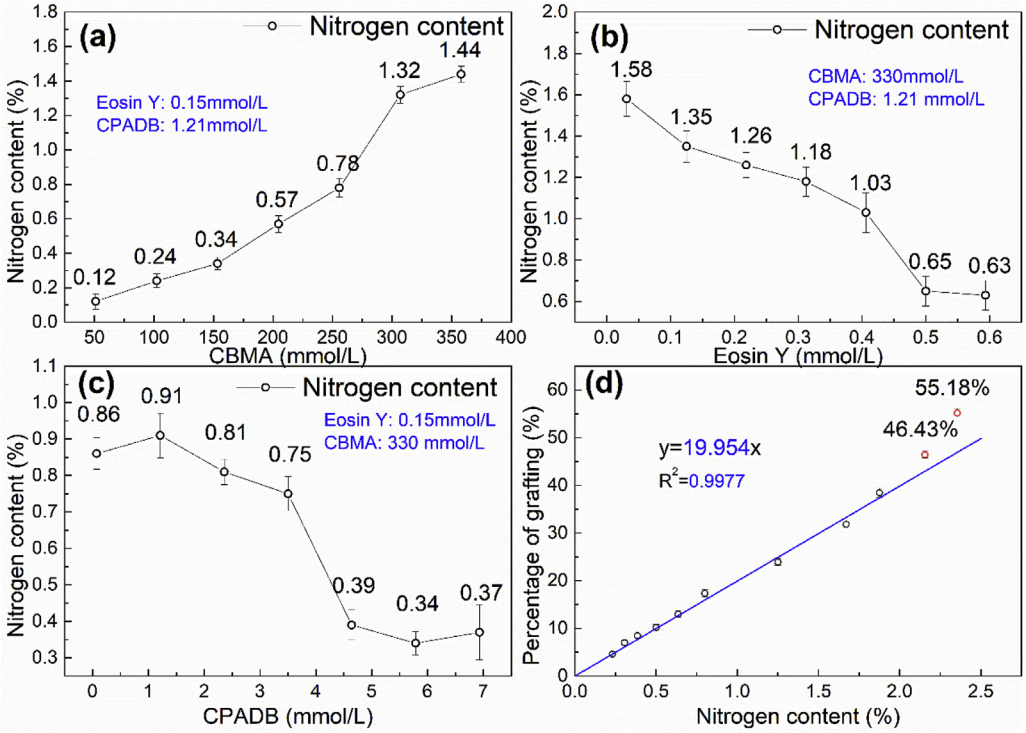


Fig. 1. Reaction factors trends of PET-RAFT process (a: CBMA; b: Eosin Y; c: CPADB) and Graft ratio conversion curve(d).

successfully, and we can get the optimal reaction conditions (CPADB: 1.20 mmol/L, eosin Y: 0.03 mmol/L and CBMA: 358 mmol/L) through control experiments.

The relationship curve between percentage of grafting and the nitrogen element content is shown in Fig. 1(d), and we can calculate the actual extent of grafting via the curve formula. While the percentage of grafting reached as high as 46.43%, it became difficult to measure the actual weight in a dry state due to its significant water absorption property of samples. Therefore, two data (percentages of grafting are 46.43% and 55.18%) upward shifted.

3.3. FTIR-ATR analysis

To investigate the chemically modification of CBMA monomer, PVA and PVA-g-pCBMA hydrogel membrane were evaluated by ATR-FTIR, as shown in Fig. 2.

Obviously, the new adsorption bands appeared at 1722 cm^{-1} and 1589 cm^{-1} are associated to the ester group (O—C=O) stretching vibrations and the carboxylate group (O=C—O^-) stretching vibrations of pCBMA polymer chains on the PVA-*g*-PCBMA hydrogel membranes, respectively [52–57].

A stronger adsorption bands at 1373 cm^{-1} is attributed to the wagging vibration of the methylene in CBMA, while another new adsorption bands at 1171 cm^{-1} attributed to methacryloyl. Besides, the weaken of the wide peak at 3280 cm^{-1} and the hypochromic shift of the peak at 918 $cm^{-1}$are attributed to the decrease of hydroxyl group (—OH) and the formation of the ether bond (C—O—C), respectively.

The ATR-FTIR results confirm that the CBMA have grafted onto the surface of PVA hydrogel membrane successfully. And it can be further confirmed by X-ray photoelectron spectroscopy (XPS).

3.4. X-ray photoelectron spectroscopy (XPS)

The survey and narrow spectrum of PVA and PVA-g-pCBMA hydrogel membrane were shown in Fig. 3. All binding energy values were determined by calibration and fixing the C-1s to 285.0 eV [58]. The

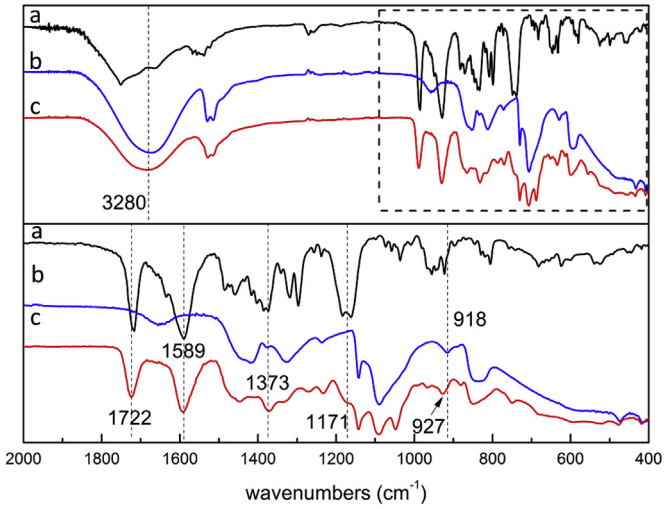


Fig. 2. FT-IR spectra of CBMA(a), ATR-FTIR of PVA(b) and PVA-g-pCBMA(c) hydrogel membrane.

major signals of C and O were observed in the survey spectrum (Fig. 3(a)) [54,55,57,59,60].

An obvious increase of nitrogen element (N-1s) can be found in the survey spectrum. Two binding energy of nitrogen can be seen in the N-1s narrow spectrum of PVA-g-pCBMA hydrogel membrane (Fig. 3(b)), C—N^+ bond in pCBMA brush with a binding energy at 402.1 eV [49] and C≡N bond in R group of CPADB with a binding energy at 399.5 eV.

The C-1s narrow spectrum (Fig. 3(d)) of PVA can be divided into two parts, 285 eV (C—C/C—H_2) and 286.5 eV (C—O/C—H) [60]. The area ratio of peak [C—C/C—H_2] and peak [C—O/C—H] is 1.29, which approached the ideal structure of PVA; while increased to 1.64 after modification. Afterward, we found it need three extra peaks to imitate the full C-1s narrow spectrum of PVA-g-pCBMA hydrogel membrane. An obvious new peak of them at 289.1 eV is stand for the O—C=O bond [57,59,60]. And according to the chemical structure of CBMA,

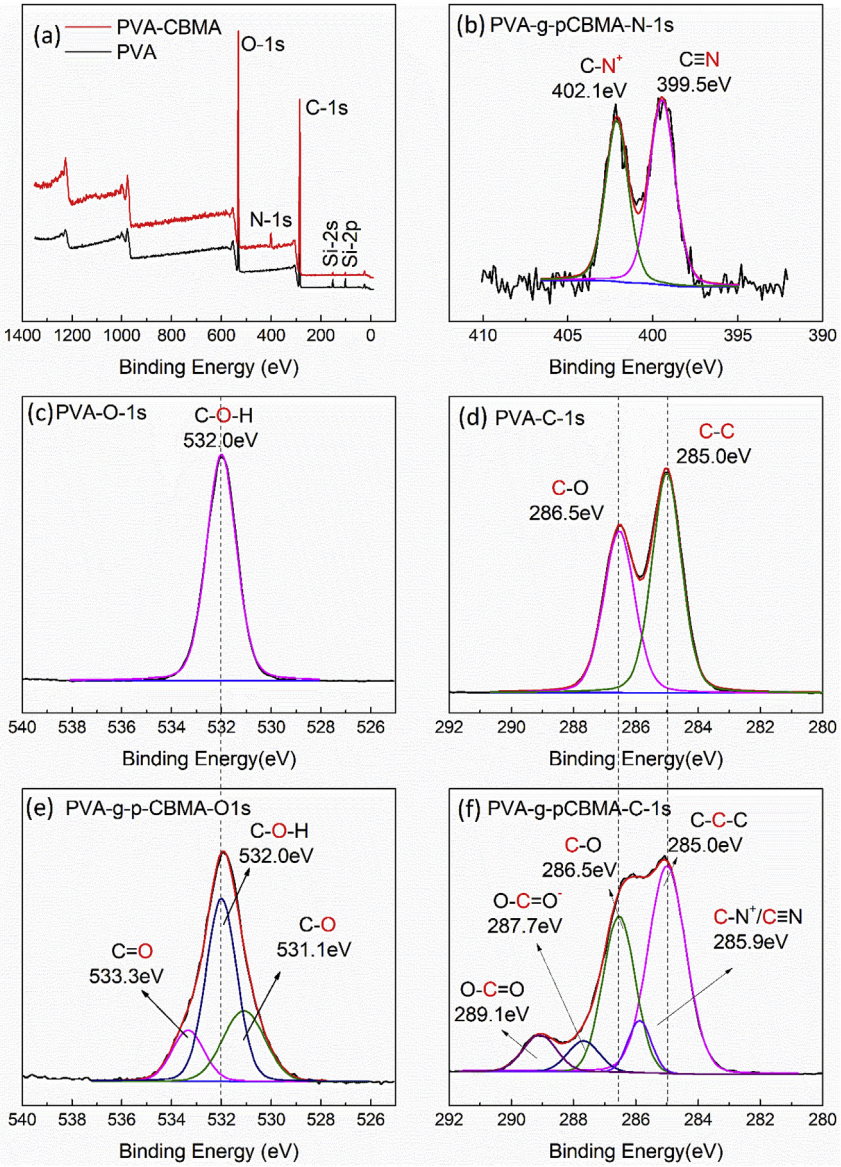


Fig. 3. XPS survey spectrum (a), C-1s narrow spectrum (d, f), N-1s narrow spectrum (b) and O-1s narrow spectrum (c, e) of the PVA and PVA-g-pCBMA hydrogel membrane surface.

additional two peaks at 287.7 eV and 285.9 eV are stand for the O=C−O$^-$ bonds and C≡N/C−N$^+$ bonds, respectively.

Due to the binding energy of O-1s in different chemical bonding are very close, few researchers have further analyzed and divided the O-1s peaks. Here, compared with O-1s narrow spectrum of PVA hydrogel membrane, the O-1s narrow spectrum (Fig. 3(e)) of PVA-g-pCBMA hydrogel membrane significantly broadened and could be divided two extra split peaks, with the binding energies at 531.1 eV and 533.3 eV, respectively. Therefore, we classified it as the [O−C=O] and [O−C=O$^-$] bond in CBMA (531.1 eV for C−O bond and 533.3 eV for C=O).

In summary, the XPS analysis has further confirmed that CBMA has been grafted onto the surface of PVA hydrogel membrane successfully.

3.5. Surface microstructure

Surface morphology of PVA and PVA-g-pCBMA hydrogel in drying state were characterized by AFM. Fig. 4 shows the AFM images of PVA and PVA-g-pCBMA hydrogel and the corresponding Ra roughness.

As shown in Fig. 4. The surface micro-topography of hydrogel in drying state has a slight change after surface grafting. The Ra roughness of hydrogel surface (3 μm × 3 μm) increased from 5.44 nm to 6.12 nm, it remained at a low level while the percentage of grafting reached at 55.18%. This result indicated that surface micro-topography of hydrogel in drying state has no striking changes after surface grafting, and the chemical composition is the main variable parameter across PVA hydrogel surface after grafting.

3.6. Ultraviolet–visible spectroscopy analysis

PVA hydrogel has a significant transmittance and we focus on whether modification process will affect its transmittance property. And Fig. 5 shows the transmittance of hydrogel membranes in different percentage of grafting.

The transmittances of samples were measured at 200–800 nm using an ultraviolet–visible spectrometer. As shown in Fig. 5, it increased ssswith the wavelength. The pristine PVA hydrogel membrane has an excellent transmittance in the range of visible light. But due to polyvinyl acetate (PVAc) is the precursors of PVA, the ester group (O−C=O) residual in PVA is unavoidable [61]. Therefore,

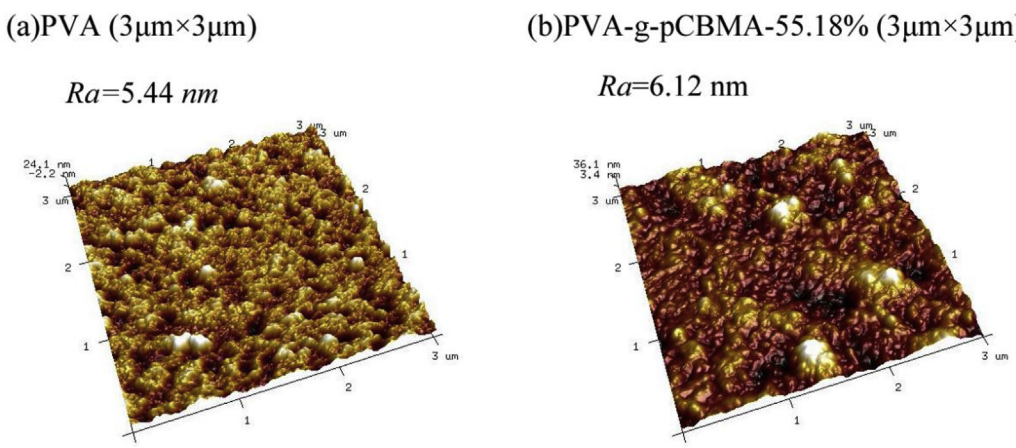


Fig. 4. Surface micro-topography in AFM (3D view).

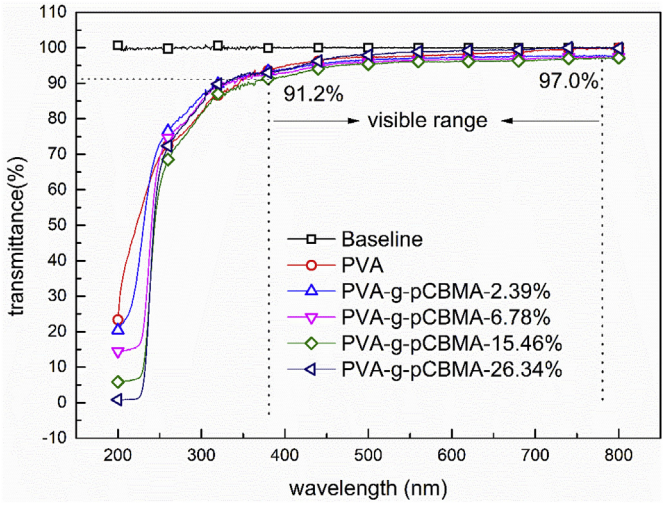


Fig. 5. Transmittance of the PVA and PVA-g-pCBMA (different percentage of grafting) hydrogel membrane.

transmittance of pristine PVA hydrogel also decreased in the range of ultraviolet light. With the increasing of percentage of grafting, transmittances of PVA-g-pCBMA hydrogel membranes remain excellent (91.2%–97.0%) in the range of visible light, while decreased regularly in the range of ultraviolet light between 200 nm–250 nm, because of C = O bond in CBMA. It also indicated that the modification process does not influence the transmittance of Hydrogel membrane in visible light range.

3.7. Thermogravimetric analysis

The thermal properties of PVA and PVA-g-pCBMA hydrogel membranes were detected by thermogravimetric analysis (TGA, 35°C-750 °C, 10 K min^{-1}).

The thermal decomposition behavior of PVA can be divided into three stages [62]. In Fig. 6, the first region (35–170 °C) has a weight loss of around 9%, cause by the evaporation of weakly bound water and non-freezing bound water. And it remains consistency between the two samples. The second transition region for pristine PVA membrane is around 170–330 °C with a weight loss of around 18%, cause by the decomposition of the hydroxyl group. PVA chain gradually changed into a kind of polymer with conjugated double bonds [63].And the third region (330–550 °C) is cause by the degradation of the polymer main chain.

Transition regions of PVA-g-PCBMA hydrogel membrane were distinguished base on the thermal curve of PVA hydrogel membrane. The first transition region remains consistency to the PVA hydrogel membrane. The second transition region is between 170 and 300 °C, with a weight loss of around 15%. And the thermal curve in this transition region higher than PVA hydrogel membrane, because the grafting sites of PVA is alkoxyl radicals. The third transition region between 300 and 366 °C is associated with the structural degradation of pCBMA brush, resulting in the apparent decrease of the thermal curve. The fourth transition region (366–550 °C, about 40% weight loss) is associated with the structural degradation of PVA and pCBMA. And the weight loss (3%) in last region slows down, may cause by the degradation of the small residual molecule in pCBMA. The residual weight percentage in 750 °C of PVA hydrogel membrane decreased to 1.27% while remaining 6.09% to the PVA-g-PCBMA hydrogel membrane. And the thermal stability of PVA-g-PCBMA hydrogel membrane below 170 °C is the same as PVA hydrogel membrane. Thus, the modification progress would not influence the application of hydrogel membrane as a biomedical material.

3.8. Hydrophilicity measurements

Swelling equilibrium, water contact angle and water content are important indexes to evaluate the hydrophilicity of materials. The swelling ratio (Q_t) and water contact angle of PVA and PVA-g-PCBMA hydrogel membrane were showed in Fig. 7(a). The hydrogel membrane is close to swelling equilibrium after immersing in ultra-pure water for 265min. Fig. 8(b) shows the moisture content of PVA-g-pCBMA hydrogel membrane in different percentage of grafting.

In Fig. 7(a), the swelling kinetics curve is similar to the lower branch of the hyperbola, according to the present hyperbola described by the formula

$$Q_{t,sample} = \frac{t}{b + a \times t} \tag{5}$$

Where a and b are the empirical constants that determine the coordinates of the center and the asymptotes of the hyperbola. Obviously, the asymptote $1/a$ is the equilibrium degree of swelling (Q_∞) in physical meaning, and two regressions coefficient can be expressed as following formula [64,65].

$$a = \frac{1}{Q_\infty}, b = \frac{t_{\frac{Q_\infty}{2}}}{Q_\infty} \tag{6}$$

where Q_∞ is the equilibrium degree of swelling and $t_{Q_\infty/2}$ is the time in semi-saturation. According to the formula above, after the mathematic calculation, the related parameters of equilibrium swelling curve are shown in Table 1.

The degree of equilibrium swelling (Q_∞) is an index to evaluate the

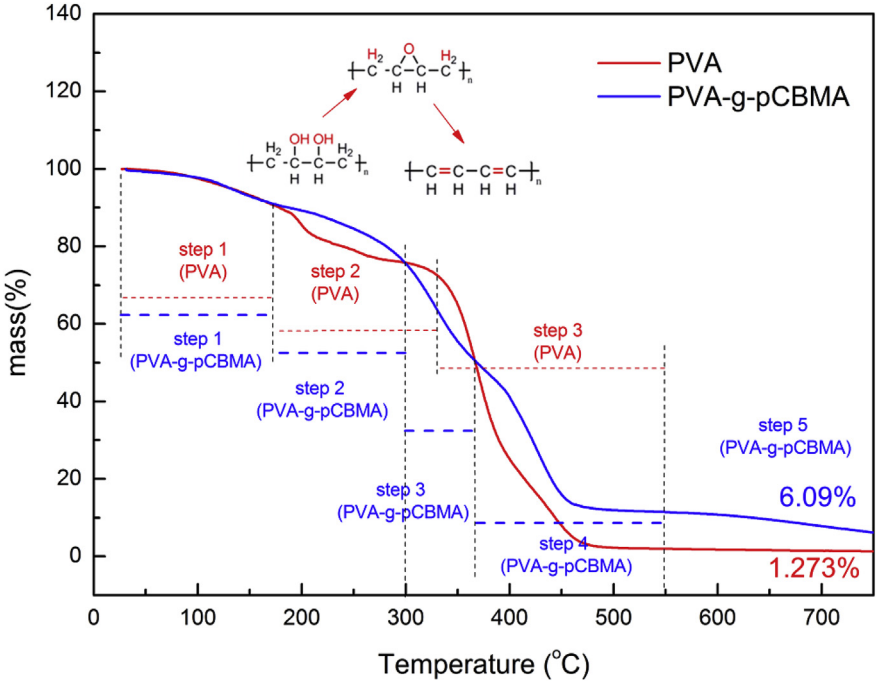


Fig. 6. The thermogravimetric of the pristine PVA and PVAg− pCBMA hydrogel membrane.

ability of water adsorption, and it increases from 2.064 $cm^3 g^{-1}$ to 3.653 $cm^3 g^{-1}$, the time in semi-saturations ($t_{Q_\infty/2}$) is to evaluate the water absorption speed of samples, and it becomes faster (from 34.20 min to 5.04 min) after grafting. Besides, water contact angle decreased from 45.94° to 18.06°.

The average water content of PVA hydrogel membrane is 67.31%, and water content of PVA-g-pCBMA hydrogel membrane increase with the increasing of percentage of grafting (Fig. 7(b)). When it reached as high as 55.18%, water content of PVA-g-pCBMA hydrogel membrane reached 78.23%.

In general, these results indicated a significant improvement of hydrophilicity of hydrogel after grafting.

3.9. Properties of anti-protein adsorption

The protein adsorption on hydrogel membrane surface will lead biofouling. The protein adsorption was assessed at λ = 562 nm using an Ultra-micro Microplate Spectrophotometer (Epoch) from a concentration standard curve ranging from 0 to 40 μg/ml.

$$y_{O.D.} = 0.0047x_c + 0.0381 (R^2 = 0.9953) \quad (7)$$

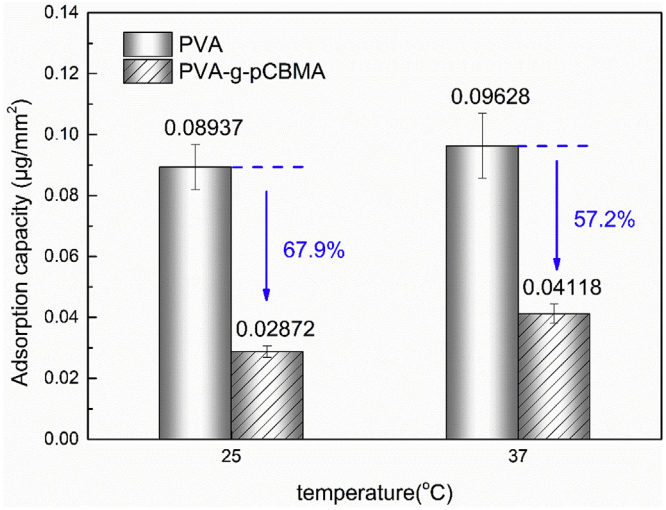


Fig. 8. Adsorption capacity of PVA and PVA-g-pCBMA hydrogel membrane.

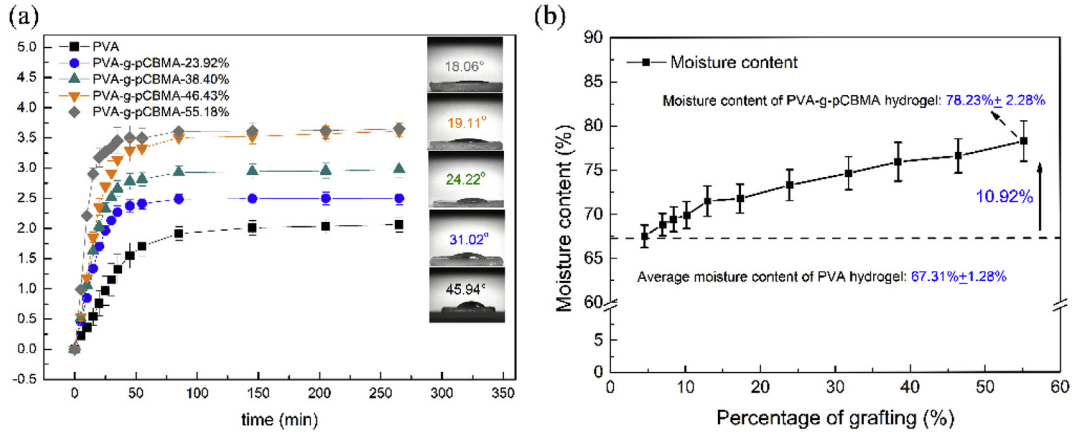


Fig. 7. Hydrophilic analysis of the PVA and PVA-g-pCBMA (different percentage of grafting) hydrogel membranes.

Table 1
The related parameters of equilibrium swelling curve.

samples	Percentage of grafting	*a*	*b*	Q_∞ / $Q_{t=265\,min}$ ($cm^3 \cdot g^{-1}$)	$t_{Q_\infty/2}$ (min)	Water contact angles
PVA	0	0.429	14.67	2.331/2.064	34.20	45.94°
PVA-g-pCBMA	23.92%	0.377	4.284	2.653/2.500	11.36	31.02°
	38.4%	0.317	3.705	3.155/2.980	11.69	24.22°
	46.43%	0.259	3.643	3.861/3.611	14.07	19.11°
	55.18%	0.267	1.346	3.745/3.653	5.04	18.06°

Where $y_{O.D.}$ is the detect value of optical density and x_c is the concentration of BSA.

The quantity of BSA protein that adsorbed on the membrane surfaces were measured, calculated and shown in Fig. 8. The amount of adsorbed protein on the surface of PVA hydrogel membrane at 25 °C was 0.0894 ± 0.00732 μg/mm^2, while reduced to 0.0287 ± 0.00191 μg/mm^2 on PVA-g-pCBMA hydrogel membrane, reduced by about 67.9%. Protein adsorption capacity of hydrogel membranes were both increased slightly at 37 °C. PVA hydrogel membrane was 0.0963 ± 0.0107 μg/mm^2, while reduced to 0.0412 ± 0.00313 μg/mm^2 after grafting, reduced by 57.2%.

Jian-hua Li et al. [66] reported a silver nanoparticle-poly (carboxybetaine methacrylate) (AgNPs-PCBMA) nanocomposite was prepared on poly (vinylidene fluoride) (PVDF) membrane surface to improve its hydrophilicity and antifouling properties. And the BSA static adsorption on the original PVDF membrane was about 752 μg/cm^2, while decreased to around 440 μg/cm^2 after grafting with pCBMA, around 41% decrease. And Shi Suqing et al. [67] grafted a hydrolysable cationic polycarboxybetaine ester polymer brush (PCBMA-1C2) onto the glass surface. And the BSA static adsorption on the original glass surface was about 0.2 μg/cm^2, while decreased by 96% on the surface of Glass-PCBMA.

Comparing the above results, we can confirm two points. First, the substrate is an important factor affecting protein adsorption, the protein adsorption of compact hard glass is as low as 0.2 μg/cm^2, while the PVDF membrane is as high as 752 μg/cm^2. As a hydrophilic polymer hydrogel membrane, the original PVA has a low protein adsorption (8.94 ± 0.732 μg/cm^2). Second, the pCBMA grafting onto surface of materials can reduce protein adsorption further, and it is an effective method to structure anti-fouling surface via pCBMA grafting.

3.10. Cytotoxicity

In order to assess the utility of PVA and PVA-g-pCBMA hydrogel membranes as biomaterials, we studied the cytotoxicity of hydrogel membrane.

As shown in Fig. 9, the relative cell viability of PVA hydrogel membrane in day1, day3 and day7 are around 95.91% ± 0.87%, 105.1% ± 2.44% and 99.93% ± 2.38%, respectively. And, relative cell viability of samples remains 90.55% ± 2.48%, 91.62% ± 2.54% and 92.81% ± 2.56% after grafted with pCBMA. According to ISO 10993-5-2016, cell viability of samples larger than 80% can be considered non-cytotoxic. Thus, both PVA and PVA-g-pCBMA hydrogel membranes can be considered as non-cytotoxic, which indicated that both of them could be used as artificial cornea material and other biomedical applications.

3.11. Anti-cell adhesion

We used eyelid fibroblasts to evaluate anti cell adhesion capacity, and the statistics data for the cell adhesion was calculated through cell count standard curve ranging from 0 to 1 × 10^5 cells/ml

$$y_{O.D.} = 0.1415x,\ R^2 = 0.9979 \quad (8)$$

Where $y_{O.D.}$ is the detect value of optical density and x is the concentration of cell suspension.

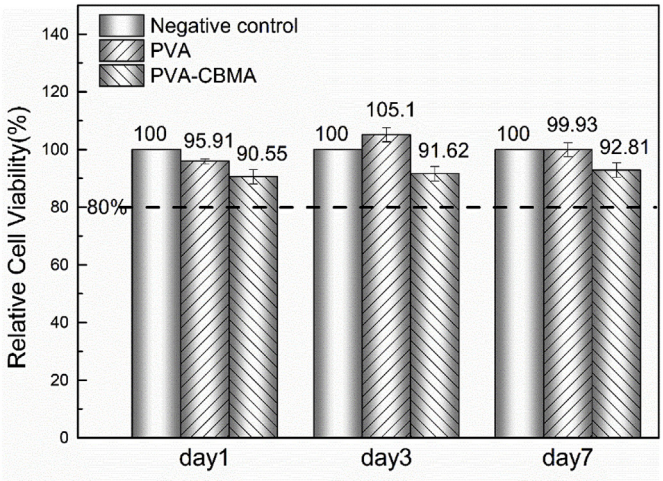


Fig. 9. Relative cell viability of PVA hydrogel and PVA-gpCBMA hydrogel membrane.

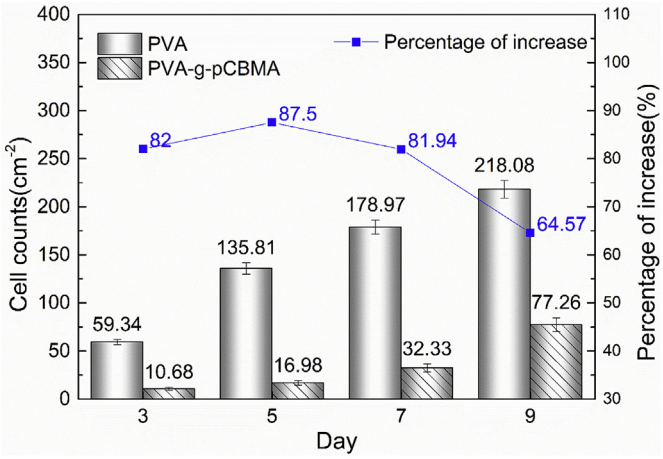


Fig. 10. Eyelid fibroblasts adhesion counts of PVA and PVA-g-pCBMA hydrogel membranes.

Fig. 10 shows the statistics data for the cell adhesion in day 1, 3, 5, 7. Due to the cell's proliferation, the quantity of cell-adhesion increases with the increasing of nurturing days. In day 7, the quantity of cell adhesion on PVA hydrogel is about 218.09 ± 9.15 cells·cm^{-2} while only 77.26 ± 7.25 cells·cm^{-2} adhered onto the surface of PVA-g-pCBMA hydrogel, which decreased by 64.57%. Therefore, it shows a great improvement in cell anti-adhesion after modification, and it is close to the anti-protein adhesion results.

Fig. 11 shows the SEM images of PVA and PVA-g-pCBMA hydrogel membrane after incubated cells. SEM images of 2000 magnification clearly showed that a significant amount of eyelid fibroblasts attached on PVA hydrogel membrane whereas only little eyelid fibroblasts on PVA-g-pCBMA hydrogel membrane.

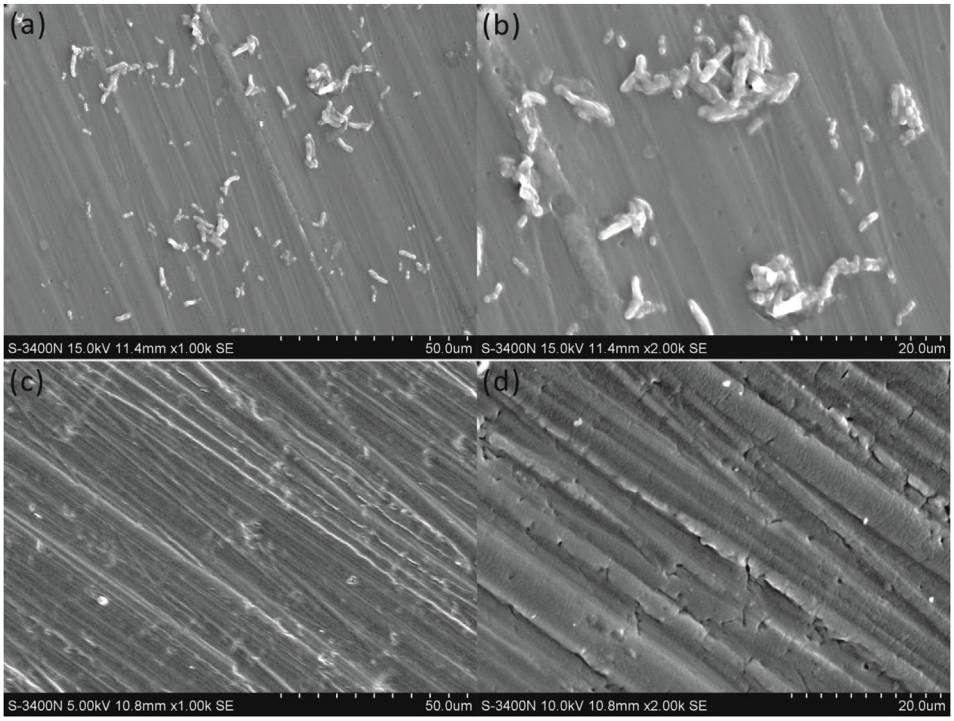


Fig. 11. Eyelid fibroblasts adhesion test (SEM, incubation for 7 days) of the PVA (a, b) and PVA-g-pCBMA (c, d) hydrogel membranes.

4. Conclusions

In this study, we immobilized the zwitterionic CBMA onto the surface of PVA hydrogel membrane via PET-RAFT to fabricate an anti-adhesion and biocompatible surface. According to ATR-FTIR spectroscopy and XPS analysis, pCBMA has been immobilized successfully onto the surface of PVA hydrogel membrane. AFM analysis showed a slight increase of Ra roughness from 5.44 nm to 6.12 nm, and it indicated the chemical composition is the main variable parameter across PVA hydrogel surface after grafting. The transmittance of PVA-g-pCBMA hydrogel membrane between visible light range (380 nm-780 nm) is 91.2%–97.0% after modification. The thermal stability below 150 °C remains consistency. Thus, the modification does not affect the basic performance of hydrogel.

On the other hand, according to hydrophilicity analysis, with the increasing of grafting from 4.58% to 55.18%, the degree of equilibrium swelling (Q_∞) increases from 2.064 $cm^3 g^{-1}$ to 3.653 $cm^3 g^{-1}$, water contact angle decreased from 45.94° to 18.06°, moisture content of hydrogel increased from 67.49% to 78.23%. Biological performance experiment results show the minimum relative cell viability is 90.55% ± 2.48%, which can be regarded as non-cytotoxic, the anti-protein adsorption capacity of PVA-g-pCBMA hydrogel increased by 67.9% at 25 °C and 57.2% at 37 °C, the anti-adhesion capacity of eyelid fibroblasts increased by 64.57%.

In summary, PET-RAFT has merits of low costs, easy realizable and low toxicity, and has a great potential to be used in introducing functional polymer brushes onto the surface of PVA hydrogel membrane and constructing functional membrane surfaces.

Conflicts of interest

There are no conflicts to declare.

Acknowledgements

This work was supported by the Shenzhen strategic emerging industry developmentfunds financed Project (NYSW 201603241024196800, NYSW20130329010039) and Sanming project medicine in Shenzhen(SZSM201512039).

Appendix A. Supplementary data

Supplementary data to this article can be found online at https://doi.org/10.1016/j.polymer.2018.12.026.

References

[1] H. Yao, J.p. Kang, W.c. Li, J. Liu, R.j. Xie, Y.j. Wang, S. Liu, D.A. Wang, L. Ren, Novel beta-TCP/PVA bilayered hydrogels with considerable physical and biofunctional properties for osteochondral repair, Biomed. Mater. 13 (1) (2017) 015012.
[2] X. Peng, C. He, J. Liu, H. Wang, Biomimetic jellyfish-like PVA/graphene oxide nanocomposite hydrogels with anisotropic and pH-responsive mechanical properties, J. Mater. Sci. 51 (12) (2016) 5901–5911.
[3] F. Delbecq, F. Kono, T. Kawai, Preparation of PVP-PVA-exfoliated graphite cross-linked composite hydrogels for the incorporation of small tin nanoparticles, Eur. Polym. J. 49 (9) (2013) 2654–2659.
[4] L.E. Millon, D.T. Padavan, A.M. Hamilton, D.R. Boughner, W. Wan, Exploring cell compatibility of a fibronectin-functionalized physically crosslinked poly(vinyl alcohol) hydrogel, J. Biomed. Mater. Res. B Appl. Biomater. 100 (1) (2012) 1–10.
[5] H. Bakhshandeh, M. Soleimani, S.S. Hosseini, H. Hashemi, I. Shabani, A. Shafiee, A.H.B. Nejad, M. Erfan, R. Dinarvand, F. Atyabi, Poly (ε-caprolactone) nanofibrous ring surrounding a polyvinyl alcohol hydrogel for the development of a biocompatible two-part artificial cornea, Int. J. Nanomed. 6 (2011) 1509–1515.
[6] E. de Souza Costa-Junior, M.M. Pereira, H.S. Mansur, Properties and biocompatibility of chitosan films modified by blending with PVA and chemically crosslinked, J. Mater. Sci. Mater. Med. 20 (2) (2009) 553–561.
[7] P.M. Kharkar, K.L. Kiick, A.M. Kloxin, Designing degradable hydrogels for orthogonal control of cell microenvironments, Chem. Soc. Rev. 42 (17) (2013) 7335–7372.
[8] J. Malda, J. Visser, F.P. Melchels, T. Jungst, W.E. Hennink, W.J. Dhert, J. Groll, D.W. Hutmacher, 25th anniversary article: engineering hydrogels for biofabrication, Adv. Mater. 25 (36) (2013) 5011–5028.
[9] Y. Zou, L. Zhang, L. Yang, F. Zhu, M. Ding, F. Lin, Z. Wang, Y. Li, "Click" chemistry in polymeric scaffolds: bioactive materials for tissue engineering, J. Contr. Release 273 (2018) 160–179.
[10] A. Kumar, S.S. Han, PVA-based hydrogels for tissue engineering: a review, Int. J. Polym. Mater. 66 (4) (2016) 159–182.
[11] W.w. Wang, Y. Lu, M.y. Luo, Q.h. Zhao, Y.d. Wang, Q.z. Liu, M.f. Li, D. Wang, Zwitterionic-polymer-functionalized poly(vinyl alcohol-co-ethylene) nanofiber membrane for resistance to the adsorption of bacteria and protein, J. Appl. Polym. Sci. 133 (44) (2016) 44169.

[12] B. Ozcelik, R. Chen, V. Glattauer, N. Kumar, M.D.P. Willcox, H. Thissen, Crosslinked platform coatings incorporating bioactive signals for the control of biointerfacial interactions, Macromol. Biosci. 17 (4) (2017) 1600315.
[13] P.A. Markov, N.S. Krachkovsky, E.A. Durnev, E.A. Martinson, S.G. Litvinets, S.V. Popov, Mechanical properties, structure, bioadhesion, and biocompatibility of pectin hydrogels, J. Biomed. Mater. Res. A. 105 (9) (2017) 2572–2581.
[14] G.R. Alas, R. Agarwal, D.M. Collard, A.J. Garcia, Peptide-functionalized poly[oligo (ethylene glycol) methacrylate] brushes on dopamine-coated stainless steel for controlled cell adhesion, Acta Biomater. 59 (2017) 108–116.
[15] A. Utrata-Wesolek, Antifouling surfaces in medical application, Polymer 58 (9) (2013) 685–695.
[16] L.f. Li, T. Nakaji-Hirabayashi, H. Kitano, K. Ohno, T. Kishioka, Y. Usui, Gradation of proteins and cells attached to the surface of bio-inert zwitterionic polymer brush, Colloids Surfaces B Biointerfaces 144 (2016) 180–187.
[17] J.J. Wang, F. Liu, Photoinduced graft polymerization of 2-methacryloyloxyethyl phosphorylcholine on silicone hydrogels for reducing protein adsorption, J. Mater. Sci. Mater. Med. 22 (12) (2011) 2651–2657.
[18] S. Chen, L.y. Li, C. Zhao, J. Zheng, Surface hydration: principles and applications toward low-fouling/nonfouling biomaterials, Polymer 51 (23) (2010) 5283–5293.
[19] H. Meng, Q. Cheng, C.x. Li, Polyacrylonitrile-based zwitterionic ultrafiltration membrane with improved anti-protein-fouling capacity, Appl. Surf. Sci. 303 (2014) 399–405.
[20] N.L. Le, M. Ulbricht, S.P. Nunes, How do polyethylene glycol and poly(sulfobetaine) hydrogel layers on ultrafiltration membranes minimize fouling and stay stable in cleaning chemicals? Ind. Eng. Chem. Res. 56 (23) (2017) 6785–6795.
[21] B.S. Lee, H.S. Shin, K. Park, D.K. Han, Surface grafting of blood compatible zwitterionic poly(ethylene glycol) on diamond-like carbon-coated stent, J. Mater. Sci. Mater. Med. 22 (3) (2011) 507–514.
[22] A. Phukon, K. Sahu, How do the interfacial properties of zwitterionic sulfobetaine micelles differ from those of cationic alkyl quaternary ammonium micelles? An excited state proton transfer study, Phys. Chem. Chem. Phys. 19 (46) (2017) 31461–31468.
[23] P.S.C. Liu, Qiang, S.S. Wu, J. Shen, S.C. Lin, Surface modification of cellulose membranes with zwitterionic polymers for resistance to protein adsorption and platelet adhesion, J. Membr. Sci. 350 (1–2) (2010) 387–394.
[24] D.s. Xiong, Y. Deng, N. Wang, Y.y. Yang, Influence of surface PMPC brushes on tribological and biocompatibility properties of UHMWPE, Appl. Surf. Sci. 298 (2014) 56–61.
[25] C. Leng, S. Sun, K. Zhang, S. Jiang, Z. Chen, Molecular level studies on interfacial hydration of zwitterionic and other antifouling polymers in situ, Acta Biomater. 40 (2016) 6–15.
[26] S.J. Zhiqiang Cao, Super-hydrophilic zwitterionic poly(carboxybetaine) and amphiphilic non-ionic poly(ethylene glycol) for stealth nanoparticles, Nano Today 7 (2012) 404–413.
[27] C.J. Huang, Y. Li, J.B. Krause, N.D. Brault, S. Jiang, Internal architecture of zwitterionic polymer brushes regulates nonfouling properties, Macromol. Rapid Commun 33 (11) (2012) 1003–1007.
[28] J. Chiefari, Y.K. Chong, F. Ercole, J. Krstina, J. Jeffery, T.P.T. Le, R.T.A. Mayadunne, G.F. Meijs, C.L. Moad, G. Moad, E. Rizzardo, S.H. Thang, Living free-radical polymerization by reversible addition-fragmentation chain transfer: the RAFT process, Macromolecules 31 (16) (1998) 5559–5562.
[29] D. Roy, J.S. Knapp, J.T. Guthrie, S. Perrier, Antibacterial cellulose fiber via RAFT surface graft polymerization, Biomacromolecules 9 (1) (2008) 91–99.
[30] J. Yuan, X. Huang, P. Li, L. Li, J. Shen, Surface-initiated RAFT polymerization of sulfobetaine from cellulose membranes to improve hemocompatibility and antibiofouling property, Polym. Chem. 4 (19) (2013) 5074-5058.
[31] J. Xu, S. Shanmugam, H.T. Duong, C. Boyer, Organo-photocatalysts for photoinduced electron transfer-reversible addition–fragmentation chain transfer (PET-RAFT) polymerization, Polym. Chem. 6 (31) (2015) 5615–5624.
[32] S. Shanmugam, J. Xu, C. Boyer, Exploiting metalloporphyrins for selective living radical polymerization tunable over visible wavelengths, J. Am. Chem. Soc. 137 (28) (2015) 9174–9185.
[33] S. Shanmugam, J. Xu, C. Boyer, Photoinduced electron transfer–reversible addition–fragmentation chain transfer (PET-RAFT) polymerization of vinyl acetate and N-vinylpyrrolidinone: kinetic and oxygen tolerance study, Macromolecules 47 (15) (2014) 4930–4942.
[34] J. Xu, K. Jung, C. Boyer, Oxygen tolerance study of photoinduced electron transfer–reversible addition–fragmentation chain transfer (PET-RAFT) polymerization mediated by Ru(bpy)$_3$Cl$_2$, Macromolecules 47 (13) (2014) 4217–4229.
[35] Y. Tsujii, M. Ejaz, K. Sato, A. Goto, T. Fukuda, Mechanism and kinetics of RAFT-mediated graft polymerization of styrene on a solid surface, Macromolecules 34 (2001) 8872–8878.
[36] Y. Zhao, S. Perrier, Synthesis of poly(methyl acrylate) grafted onto silica particles by Z-supported RAFT polymerization, Macromol. Symp. 248 (1) (2007) 94–103.
[37] D. Roy, J.S. Knapp, J.T. Guthrie, S. Perrier, Antibacterial cellulose fiber via RAFT surface graft polymerization, Biomacromolecules 9 (2008) 91–99.
[38] D. Roy, J.T. Guthrie, S.b. Perrier, Graft polymerization: grafting poly(styrene) from cellulose via reversible addition-fragmentation chain transfer (RAFT) polymerization, Macromolecules 38 (2005) 10363–10372.
[39] D. Roy, Controlled modification of cellulosic surfaces via the reversible addition–-fragmentation chain transfer (RAFT) graft polymerization process, Aust. J. Chem. 59 (2006) 229.
[40] Y. Li, H. Xue, Y. Song, Production and Purification of Carboxylic Betaine Zwitterionic Monomers, Zwitter Technology, LLC, United States, 2014.
[41] J. Phommalysack-Lovan, Y. Chu, C. Boyer, J. Xu, PET-RAFT polymerisation: towards green and precision polymer manufacturing, Chem. Commun. 54 (50) (2018) 6591–6606.
[42] K. Tu, T.c. Xu, L.f. Zhang, Z.p. Cheng, X.l. Zhu, Visible light-induced PET-RAFT polymerization of methacrylates with novel organic photocatalysts, RSC Adv. 7 (39) (2017) 24040–24045.
[43] M.R. Hill, R.N. Carmean, B.S. Sumerlin, Expanding the scope of RAFT polymerization: recent advances and new horizons, Macromolecules 48 (16) (2015) 5459–5469.
[44] J. Zhang, Y. Chen, Visible-light-induced carboxyl and alkoxyl radical generations and reactions, Hua Hsueh Hsueh Pao 75 (2017) 41–48.
[45] Q. Liu, Z. Liu, Application of photo-induced electron transfer reactions to organic synthesis, Chin. J. Org. Chem. 29 (3) (2009) 380–391.
[46] H.G. Yayla, H. Wang, K.T. Tarantino, H.S. Orbe, R.R. Knowles, Catalytic ring-opening of cyclic alcohols enabled by PCET activation of strong O-H bonds, J. Am. Chem. Soc. 138 (34) (2016) 10794–10797.
[47] D.A. Nicewicz, D.W.C. MacMillan, Merging photoredox catalysis with organocatalysis: the direct asymmetric alkylation of aldehydes, Science 322 (2008) 77–81.
[48] J.M. Narayanam, C.R. Stephenson, Visible light photoredox catalysis: applications in organic synthesis, Chem. Soc. Rev. 40 (1) (2011) 102–113.
[49] M. Semsarilar, S. Perrier, 'Green' reversible addition-fragmentation chain-transfer (RAFT) polymerization, Nat. Chem. 2 (10) (2010) 811–820.
[50] J.C. Foster, S.C. Radzinski, J.B. Matson, Graft polymer synthesis by RAFT transfer-to, J. Polym. Sci., Polym. Chem. Ed. 55 (18) (2017) 2865–2876.
[51] A.J. Gormley, J. Yeow, G. Ng, O. Conway, C. Boyer, R. Chapman, An oxygen-tolerant PET-RAFT polymerization for screening structure-activity relationships, Angew. Chem. Int. Ed. 57 (6) (2018) 1557–1562.
[52] J. Wang, Z. Wang, J.x. Wang, S.c. Wang, Improving the water flux and bio-fouling resistance of reverse osmosis (RO) membrane through surface modification by zwitterionic polymer, J. Membr. Sci. 493 (2015) 188–199.
[53] B.L. Leigh, E. Cheng, L.j. Xu, C. Andresen, M.R. Hansen, C.A. Guymon, Photopolymerizable zwitterionic polymer patterns control cell adhesion and guide neural growth, Biomacromolecules 18 (8) (2017) 2389–2401.
[54] Q. Zhou, X.P. Lei, J.H. Li, B.F. Yan, Q.Q. Zhang, Antifouling, adsorption and reversible flux properties of zwitterionic grafted PVDF membrane prepared via physisorbed free radical polymerization, Desalination 337 (2014) 6–15.
[55] Y. Wei, J.x. Zhang, X.t. Feng, D.y. Liu, Bioactive zwitterionic polymer brushes grafted from silicon wafers via SI-ATRP for enhancement of antifouling properties and endothelial cell selectivity, J. Biomater. Sci. Polym. Ed. 28 (18) (2017) 2101–2116.
[56] G. Mahmud, S. Huda, W. Yang, K. Kandere-Grzybowska, D. Pilans, S.y. Jiang, B.A. Grzybowski, Carboxybetaine methacrylate polymers offer robust, long-term protection against cell adhesion, Langmuir : the ACS journal of surfaces and colloids 27 (17) (2011) 10800–10804.
[57] H. Wang, G. Yue, C. Dong, F. Wu, J. Wei, Y. Yang, Z. Zou, L. Wang, X. Qian, T. Zhang, B. Liu, Carboxybetaine methacrylate-modified nylon surface for circulating tumor cell capture, ACS Appl. Mater. Interfaces 6 (6) (2014) 4550–4559.
[58] M. Kazemi Ashtiani, M. Zandi, P. Shokrollahi, M. Ehsani, H. Baharvand, Surface modification of poly(2-hydroxyethyl methacrylate) hydrogel for contact lens application, Polym. Adv. Technol. 29 (4) (2018) 1227–1233.
[59] Y.l. Sun, C.l. Chen, H. Xu, K. Lei, G.z. Xu, L. Zhao, M.d. Lang, Surface modification of silicon wafer by grafting zwitterionic polymers to improve its antifouling property, Appl. Surf. Sci. 419 (2017) 642–649.
[60] W.J. Yang, K.-G. Neoh, E.-T. Kang, S.L.-M. Teo, D. Rittschof, Stainless steel surfaces with thiol terminated hyperbranched polymers for functionalization via thiol-based chemistry, Polym. Chem. 4 (2013) 3105–3115.
[61] Y. Li, J. Deng, J. Zhang, A new-style poly(vinyl alcohol) gel prepared by automatic hydrolysis of poly(vinyl acetate) emulsion, J. Appl. Polym. Sci. 135 (47) (2018) 46853.
[62] S.X. Haigang Yang, Long jiang and yi dan, thermal decomposition behavior of poly (vinyl alcohol) with different hydroxyl content, J. Macromol. Sci. 51 (2012) 464–480.
[63] G. Guerrero, M.-B. Hägg, G. Kignelman, C. Simon, T. Peters, N. Rival, C. Denonville, Investigation of amino and amidino functionalized Polyhedral Oligomeric SilSesquioxanes (POSS®) nanoparticles in PVA-based hybrid membranes for CO_2/N_2 separation, J. Membr. Sci. 544 (2017) 161–173.
[64] A.D. Drozdov, A.A. Papadimitriou, J.H.M. Liely, C.G. Sanporean, Constitutive equations for the kinetics of swelling of hydrogels, Mech. Mater. 102 (2016) 61–73.
[65] S. Jana, J. Ray, S.K. Bhanja, T. Tripathy, Removal of textile dyes from single and ternary solutions using poly(acrylamide-co-N-methylacrylamide) grafted katira gum hydrogel, J. Appl. Polym. Sci. 135 (10) (2018) 45958.
[66] D.-b.Z. Jian-hua Li, Xing-xing Ni, Hui Zheng, Qi-qing Zhang, Excellent hydrophilic and anti-bacterial fouling PVDF membrane based on Ag nanoparticle self-assembled PCBMA polymer brush, Chin. J. Polym. Sci. 35 (7) (2017) 809–822.
[67] Z.Y. Shi Suqing, Qin Zhang, Na Gao, Yang Yang, Yongkuan Gong, Fabrication and surface properties of hydrolyticly function-switchable polymer brush, Chem. J. Chin. Univ. 35 (5) (2014) 1093–1099.